International Journal of Mechanical and Electrical Engineering
ISSN: 3005-9615 (Print), ISSN: 3005-7132 (Online) | Volume 6, Number 1, Year 2025
DOI: https://doi.org/10.62051/ijmee.v6n1.07
Journal homepage: https://wepub.org/index.php/IJMEE/index

Numerical Study on the Screening Performance of a Cylindrical Vibrating Screen with Coupled Rotation and Vibration

Yujia Li [1,*], Yu Xia [1], Tao Ren [2], Weiye Zhuang [1], Zheyi Jin [1], Weisong Yu [1], Xiao Huang [1]

[1] School of Mechatronic Engineering, Southwest Petroleum University, Chengdu, China

[2] State Key Laboratory of Geohazard Prevention and Geoenvironmental Protection, and School of Mechanical and Electrical Engineering, Chengdu University of Technology, Chengdu 610059, China

* Corresponding author: Yujia Li (Email: yujiali321@foxmail.com)

ABSTRACT

Advancements in drilling technology and the increasing demand for complex drilling fluids have revealed the limitations of conventional solid control systems, driving the need for innovation. This paper proposes a cylindrical vibrating screen with coupled rotation and vibration, which improves solid-liquid screening efficiency and large particle agglomeration compared to traditional planar screens. The efficiency of a vibrating screen depends on factors such as frequency, rotational speed, amplitude, and inclination angle, making optimization of these parameters critical for enhancing industrial production efficiency. Using the Discrete Element Method (DEM), this study simulates wet and dry particle screening on a cylindrical vibrating screen. It evaluates particle screening efficiency, collision frequency, and particle distribution across 30 different vibration parameter combinations. The analysis identifies the optimal settings for frequency, amplitude, speed, and inclination angle under various conditions. The optimal combination was found to be an amplitude of 4 mm, frequency of 15 Hz, rotational speed of 10 rpm, and a screen inclination angle of 0°. Screening efficiency is higher when particles exhibit an arithmetic distribution on the screen. This study provides valuable insights for the efficient operation and optimal design of cylindrical vibrating screens.

KEYWORDS

Rotation and Vibration; Cylindrical; Vibrating Screen; Discrete Element Method; Screening Efficiency.

1. INTRODUCTION

With the increase in drilling depth and the development and implementation of new drilling techniques, the use of high-density, high-viscosity fluid and drilling fluid has become inevitable, rendering the existing conventional multi-stage solid-phase control systems increasingly inadequate. Conventional oil drilling screens are planar vibrating screens, which have certain limitations in processing the new drilling fluid. Additionally, drum screens used in the mining industry only exhibit rotary motion, leading to easy clogging of screen holes and low screening efficiency. The recycling of particles after vibration screening needs to be paid close attention to. There is an urgent need to develop solidphase control equipment and systems with better processing efficiency. The authors proposed a new drilling fluid solid control system, consisting of a multi-layer ultra-wide screen surface translational elliptical drilling vibrating screen, an integrated solid-liquid separator, and a large-capacity centrifuge as the core components, to replace the existing multi-stage solid-phase

control systems (Li, Fang, and Zhang 2019). One of the integrated solid-liquid separators is the cylindrical vibrating screen with coupled rotation and vibration studied in this article. The efficiency of screening by a vibrating screen is heavily dependent on vital factors like rotational speed, frequency, amplitude, and the inclination of the screen, which are closely tied to industrial production efficiency. Therefore, careful design and optimization of these screening equipment parameters is crucial (Y Li et al. 2021; Wang et al. 2020; Wu et al. 2024; Elskamp et al. 2015; Ning et al. 2019; Yin et al. 2022; Makinde et al. 2015).

The intricate dynamics of particle motion in screening arise from their interactions and contact with the screen (Asbjornsson et al. 2016). For cylindrical vibrating screens, it is challenging to explore the detailed effect of these parameters related to the screening effect through experimental methods. Currently, research on vibrating screens focuses primarily on the analysis of screening results (Jiang et al. 2017). The screening process is not wellunderstood in existing research, and there is a particular lack of thorough studies on cylindrical vibrating screens. Conventional experimental methods have limitations in capturing and analyzing the screening process and are often accompanied by high costs (Zhao et al. 2017; Shanmugam et al. 2023; M Li 2020).

Numerical simulation techniques based on the Discrete Element Method (DEM) are capable of simulating virtual screening tests and thus predicting ideal screening operating parameters without performing actual physical tests (Cleary 2004; Elskamp et al. 2016). It has been widely used in several fields of science and technology such as mineral processing, chemical engineering, applied physics, and agricultural engineering (Zhu et al. 2008; Zadravec et al. 2018; Zhong et al. 2016; Z Li et al. 2019; Wu et al. 2018; Chen et al. 2019; Tang et al. 2020).

Dong et al. (2013) investigated the effect of linear, circular, and elliptical vibration modes on the screening process. Liu et al. (2013) studied the movement of particles on a single-deck banana screen and concluded that the screening effect does not significantly improve when the banana screen length exceeds 430 mm. Chen et al. (2021) investigated the drive frequencies of the two motors for a two-motor-driven elliptical vibrating screen, revealing the significant effect of different drive frequencies on the vibration direction angle of the self-synchronized system. Safranyik et al. (2019) studied the motion of individual spherical particles in the non-inertial frame of reference of a vibrating screen and used analytical methods to determine optimal vibration parameters for the vibrating screen. Yang et al. (2022) used DEM simulation to optimize the screening efficiency of a linear vibrating screen for recycled asphalt pavement.

In previous studies, The authors thoroughly examined the dynamic features and synchronous drive concepts of large multi-deck vibrating screens, leading to the development of a dynamic model for a two-motor flexible drive vibration system. The model not only optimizes the force conditions but also enhances the excitation force of the vibrating screen, which lays an important foundation for the study of the excitation source of the cylindrical vibrating screen with coupled rotation and vibration in this paper (Y Li et al. 2020; Y Li et al. 2019). However, the new cylindrical vibrating screen with coupled rotation and vibration proposed in this paper differs from conventional single-motion screening equipment. The research delves deeply into how structural design and vibration parameters impact screening performance, playing a pivotal role in the development and enhancement of equipment efficiency.

This paper investigates the screening process of cylindrical vibrating screens using DEM, focusing on how rotational speed, amplitude, frequency, and screen inclination angle impact screening performance. It also examines particle agglomeration at the end of the screening process, which plays a role in solid-phase recycling. The study analyzes screening efficiency and particle-screen collisions across 30 sets of varying surface energy, considering the combined effects of vibration parameters on screening efficiency. Several optimal parameter combinations for different conditions are identified. Additionally, the impact of particle distribution on the screen's efficiency is explored. The findings

contribute to improving cylindrical vibrating screen design and offer valuable insights for enhancing its operation and optimization.

2. NUMERICAL EXPERIMENTS

2.1. Contact Model

The nature of interactions differs between various substances. Establishing the contact model for both particle-particle interactions and particle-screen interactions is important. The contact model details the interactions between elements that come into connect with one another. To simulate normal contact, the Hertz-Mindlin (no-slip) model was applied, known for its accuracy and efficiency in force calculations. Figure 1. shows that the Hertz-Mindlin (no-slip) model was used to model the dry particles. The Hertz-Mindlin (no-slip) model with JKR (Johnson-Kendall-Roberts) cohesion was applied to model wet particles. In this paper, the presented model is employed to simulate the behavior of wet particles within the context of solids control, leveraging the theoretical foundation established by Mindlin and Deresiewicz. The model incorporates the effects of van der Waals forces within the contact region, thereby enhancing the precision of the simulation by accounting for these fundamental intermolecular interactions Xu et al. 2022.

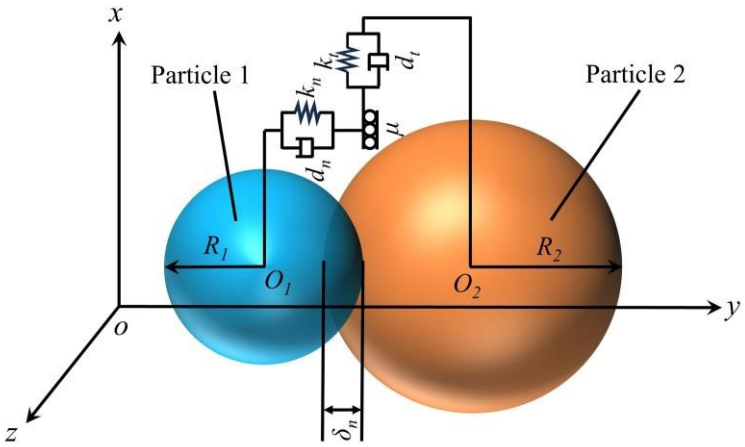

Figure 1. Hertz–Mindlin (no-slip) contact model.

Due to the wet nature of the particles, cohesive forces can be observed between them even if they are not physically touching. The maximum gap δ_c between particles under non-zero forces is:

$$\delta_c = \sqrt{-4\pi\gamma a_c I E^*} + \frac{a^2_c}{R^*} \tag{1}$$

$$a_c = \left[\frac{9\pi\gamma R^{*2}}{2E^*}\left(\frac{3}{4} - \frac{1}{\sqrt{2}}\right)\right]^{\frac{1}{3}} \tag{2}$$

Where E*, R*, γ, a, ac and δ are the equivalent Young's modulus, the equivalent radius, the energy of the particle's surface, the distance between particles, and the magnitude of normal overlap between particles, respectively. When $\delta < \delta_c$, the model is subjected to zero force.

The maximum cohesive force occurs when the particles are not in contact, and the separation gap is less than δ_c. The maximum cohesive force is called the pull-out force. The magnitude of the maximum cohesive force F_{P1} is known as the resistance to pull-out and can be expressed as

$$F_{P1} = -\frac{3}{2}\pi\gamma R^* \tag{3}$$

The separation force between particles F_{P2} is contingent upon the liquid's surface tension and the wetting angle θ. We have

$$F_{P2} = 2\pi\gamma_s \cos(\theta)\sqrt{R_1 R_2} \tag{4}$$

2.2. Force Analysis of Particles in a Cylindrical Vibrating Screen

A portion of the screen is selected as the object of study, and a coordinate system is established as shown in Figure 2, which is fixed to the screen box, meaning the coordinate system does not rotate with the screen. Applying Newton's laws of mechanics, the force analysis of the particles reveals that they are subjected to gravity, screen support force, friction forces along the radial directions r , axial directions z , and tangential directions τ, and inertia force. The following outlines the forces applied to the particles in the three coordinate directions:

$$\begin{cases} P_\tau = P_{f\tau} - G_\tau - m(a_\tau + \Delta\tau) \\ P_r = G_r + F_r - m(a_r + \Delta r) - N \\ P_y = P_{fy} - G_y - m(a_y + \Delta y) \end{cases} \tag{5}$$

Where N is the support force of the particles on the screen surface, in Newtons (N); m is the mass of the particles, in kilograms (Kg); rT is the radius of the cylindrical screen, in meters (m); ωy is the rotational angular velocity of the cylindrical screen radius, in radians per second (rad/s); Fr is the centrifugal inertia force of the particles, in Newtons (N); Pτ, Pr, Py, are the tangential, radial, and axial forces, in Newtons (N); P fτ P fy, are the friction in the tangential direction and friction in the axial direction, in Newtons (N); aτ, ar, ay are the acceleration components of vibration acceleration in the tangential, radial, and axial directions, respectively, in meters per second squared (m/s²); Gτ, Gr, Gy are the components of gravity along the tangential, radial, and axial directions, in Newtons (N); and Δτ, Δr, Δy indicates the acceleration of particles relative to the screen surface, encompassing the tangential, radial, and axial directions, respectively, in meters per second squared (m/s²).

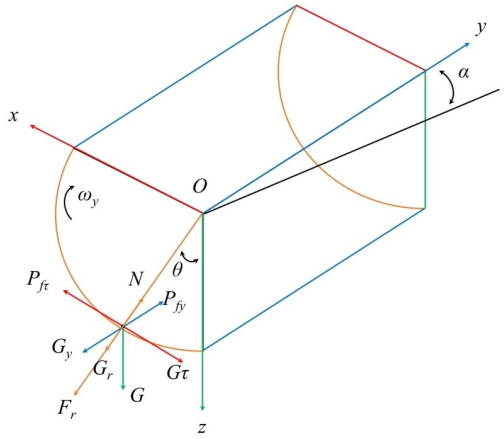

Figure 2. Force on particles on a cylindrical screen.

2.3. Definition of Screening Efficiency

Comparison of the number of particles before and after screening is critical in assessing the effectiveness of screening. This paper introduces the concept of particle screening efficiency to more clearly demonstrate the effects of different factors on the particle screening process.

Particle screening efficiency can be measured by calculating the ratio of the number of effective particles separated by the vibrating screen to the total number of effective particles produced (Yin, Zhang, and Han 2016; Zhao et al. 2017). The higher the efficiency of effective particle screening, the greater the final particle screening efficiency. The final particle screening efficiency is

$$\rho_L = \frac{N_L}{N_T} \times 100\% \tag{6}$$

where N_L is the quantity of particles that pass through the screen and N_T is the aggregate number of effective particles created.

3. MODEL AND PARAMETER SETTINGS

The complete model of the cylindrical vibrating screen has been constructed. However, as shown in Figure 3, analysis using EDEM 2022 software is infeasible due to the model's complexity. Additionally, only the side plates and sieve surface significantly impact particle movement. Thus, to reduce complexity, less critical components were excluded from this study, resulting in the simplified model displayed in Figure 4.

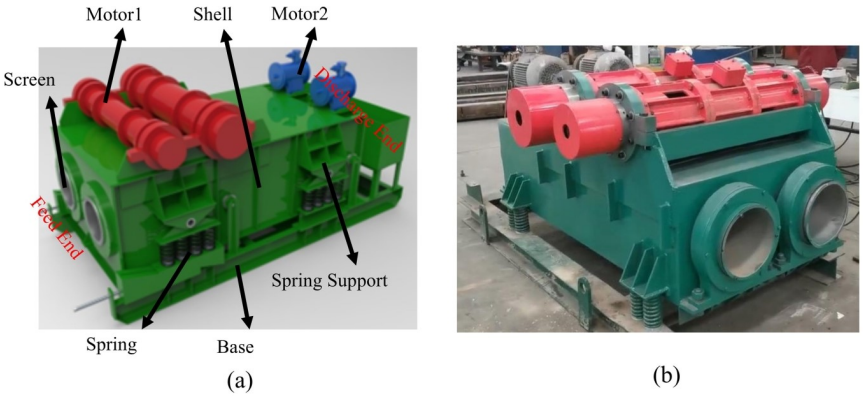

Figure 3. (a) Complete model; (b) Prototype of the screen.

As shown in Figure 4, The mesh size of the cylindrical vibrating screen is 200 mesh, with a grid size of 0.85 mm. The proportional reduction method was applied in the calculations to improve the computational efficiency of the simulation. This method reduces model complexity by ignoring the less critical parts of the vibrating screen. During the numerical simulation process, only the box and the screen are considered. The dimensions of the screen are 200 mm in length and 13 mm in diameter. The particles have a certain initial velocity when entering the screen from the particle source. During screen movement, small particles are able to pass through the holes, while larger particles remain on the screen surface. The particle generation rate was 8000 particles/s. The total duration of the simulation was 2 seconds, during which 16,000 particles were produced.

Considering the complexity of the simulation process, this simulation simplifies the modeling of the particles, which are all spherical. Table 1 presents the physical parameters associated with the particles and the screen. Interactions are defined to describe the behavior of materials when they come into contact with one another. Table 2 displays the interactions of all materials within the model. The surface energies were set at 0.5 J/m², 1 J/m², 1.5 J/m², and 2 J/m², and the effects of different surface energies on various combinations of parameters were compared. The impact of rotational speed, vibration frequency, inclination angle on particle screening performance and amplitude is analyzed. To study the effects of these four parameters, the simulation used the control variable method, changing one parameter individually. Table 3 displays the selected simulation parameters. Since the trend of screening efficiency is not obvious when the amplitude is between 2 mm and 5 mm at 0.5 J/m² surface energy, two more data sets of 6mm and 7 mm amplitude were measured relative to 0 J/m² surface energy.

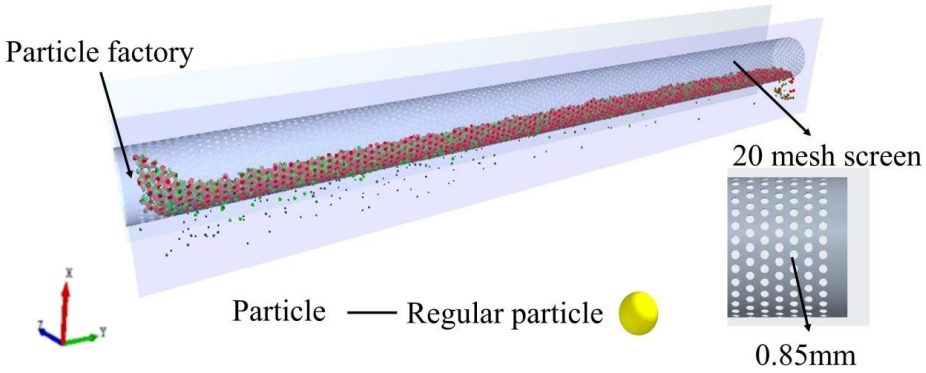

Figure 4. 3D model of cylindrical vibrating screen.

Table 1. Material parameters.

Material performance	Poisson's Ratio	Density	Shear Modulus
particles	0.2	2600kg/m^3	50MPa
screen	0.3	7800kg/m^3	70GPa

Table 2. Interactions of materials.

Material	Coefficient of recovery	Coefficient of static friction	Coefficient of rolling friction
Particles and particles	0.0003	0.44	0.01
Particles and screen	0.03	0.5	0.002

Table 3. Simulation parameters.

Surface energy (J/m^2)	Frequency (Hz)	Amplitude (mm)	Speed (rpm)	Inclination angle (°)
0	15, 20, 25, 30	2, 3, 4, 5	10, 20, 30, 40, 50	0, 1, 2, 3
0.5	15, 20, 25, 30	2, 3, 4, 5, 6, 7	10, 20, 30, 40, 50	-

4. RESULTS AND DISCUSSION

4.1. Impact Analysis

The DEM results clearly indicate a significant impact on the screen surface, with excessive impact forces potentially leading to screen breakage and disrupting the normal operation of the vibrating screen. Due to the random positioning of particles, only a portion are in contact with the sieve surface at any given time. Considering the instantaneous impact force at a single moment does not capture the cumulative effect of all particles on the screen surface, nor the full stress distribution across it. Therefore, this study examines the impact over a period, allowing observation of stress changes as material spreads across the surface throughout the screening process.

Table 5 presents the analysis results, highlighting variations in impact force and stress during screening. As particle quantity increases, impact forces also rise, leading to greater stress on the screen

surface. Due to a lack of support in the center, this area experiences significantly higher stress, making it susceptible to damage under strong alternating loads. Thus, positioning a support beam in the middle of the screen is essential for reducing stress and enhancing the screen's structural reliability.

Table 4. Experimental results of DEM analysis.

Item			Time(s)		
	0-0.5	0.5-1		1-1.5	1.5-2
Impact force($\times 10^{-3}$N)	14.92	15.02		16.23	17.69
Maximum stress(KPa)	221.051	469.71		500.84	544.62

4.2. Effect of Different Surface Energy on Particle Screening Efficiency

For the purpose of screening high-density drilling fluids, this article presents a cylindrical vibrating screen as a proposed solution. The paper investigates the vibration parameters related to vibrating screens. To reduce complexity in the research process, the viscosity between particles was represented by surface energy (Biresaw and Carriere 2001). A material's capacity to retain moisture on its surface is described by surface energy, which also affects adhesion (Steffen et al. 2018). The simulation of the movement of wet particles on the screen is controlled by setting the surface energy. The adhesive nature of wet particles causes smaller particles to attach to larger ones or form aggregates through surface adhesion (Johnsin, Kendall, and Roberts 1971). Surface energies were obtained considering the physical properties of the drilling fluid, modeled particle shapes, and the GEMM (Liao et al. 2021; Zhai, Xiong, and Tang 2019). As shown in Figure 5(a), increased surface energy results in a lower average frequency of particle impacts with the screen. As shown in Figure 6, during the vibration process, due to the existence of surface energy, the particles have a certain degree of moisture on their surfaces, causing the wet particles to adsorb other nearby wet particles, leading to the particles sticking together.

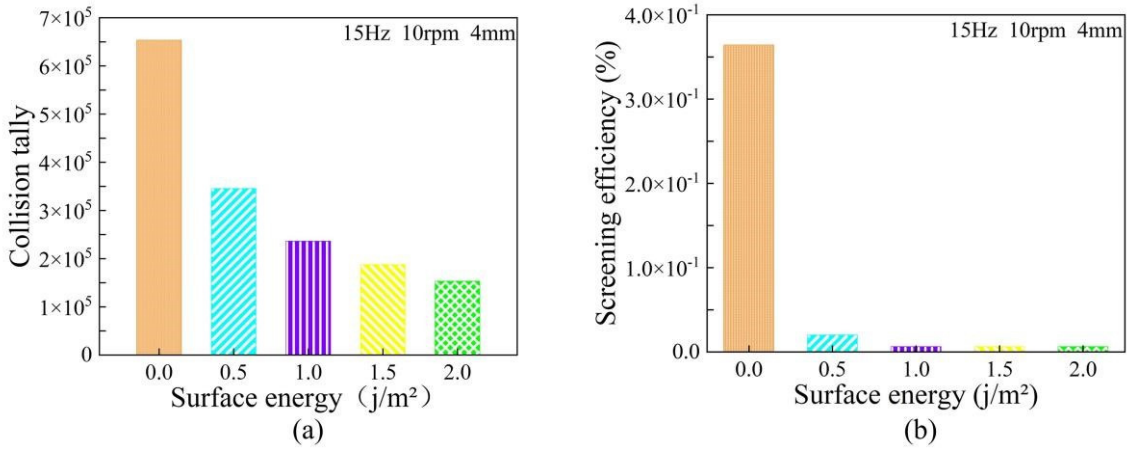

Figure 5. (a) Collision tally at different surface energies; (b) Screening efficiency at different surface energies.

The average collision tally between the particles and compared to a surface energy of 0 J/m², a surface energy of 0.5 J/m² led to a 47.1% decrease in the screening surface. The average collision tally at a surface energy of 2 J/m² was 23.47% of that at 0 J/m². As shown in Figure 5(b), the screening efficiency of the particles at a surface energy of 0.5 j/m² was 5.52% of that at 0 j/m². At a surface energy of 2 J/m², the screening efficiency fell to 1.7% of the efficiency observed at 0 J/m². An increase in the water content of particles leads to a higher viscosity in the mixed phase fluid. The increased

interaction of wet particles strengthens the adhesion between them and the screen holes. When moving on the screen surface, wet particles exhibit a smaller rebound phenomenon than those with lower water content. Additionally, the attachment of small particles to larger ones results in reduced particle penetration. Lastly, we will evaluate the differences in particle screening efficiency generated by different vibration parameter combinations for surface energies of 0 J/m² and 0.5 J/m².

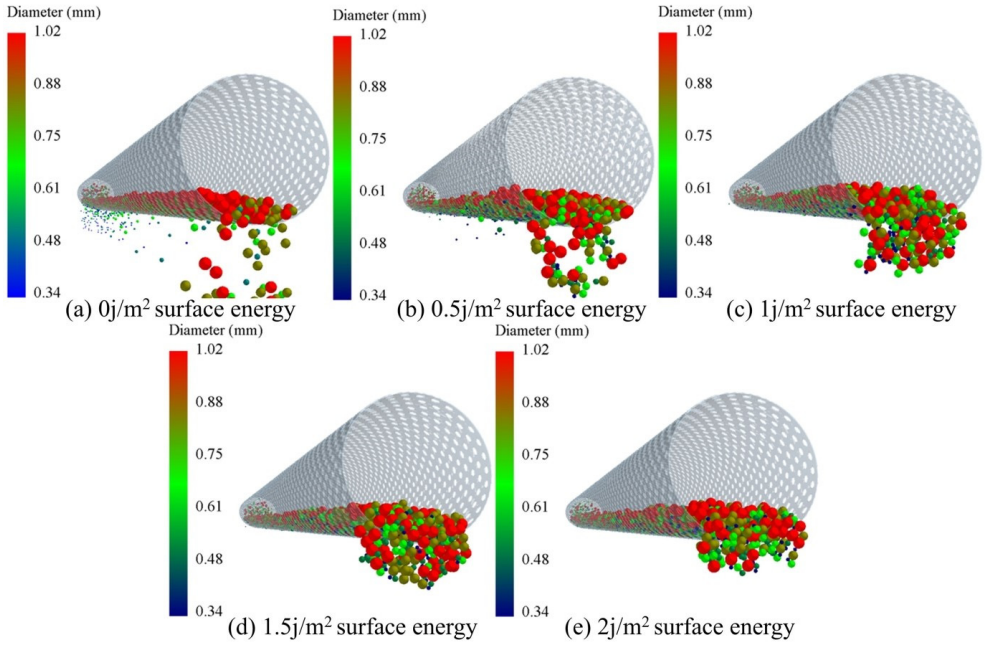

Figure 6. Particle sticking at 1.4 s for different surface energies.

Therefore, in the vibrating screening process, dehumidifying the screening object is an essential part of improving particle screening efficiency. During screening, the rotary movement of the cylindrical vibrating screen helps to dehumidify the particles. When particles become lodged in the screen, it is difficult to unlock the screen if it only has rotary motion. The rotational variation of the equalized elliptical motion force within one plane makes it easier to unlock stuck particles.

4.3. Effect of Screen Structure and Vibration Parameters on Particle Screening Efficiency

(1) Effects of parameters on screening efficiency at the surface energy is 0 J/m².

As shown in Figure 7(a), The screening efficiency is highest among all parameter combinations when the rotational speed is 10 rpm, the screen surface angle is 0°, amplitude is 4 mm, and frequency is 15 Hz. At a screen inclination of 0°, it takes 1.15 seconds for the particles to reach the outlet. At a screen inclination of 1°, the time for particles to reach the outlet is 3% higher than at an inclination of 0°; At a screen inclination of 2°, particles reach the exit 6% slower than at an inclination of 0°; At a screen inclination of 3°, the time for particles to reach the outlet is 10% higher than at an inclination of 0°. When the screen has a certain angle of inclination, the particles will appear to climb with the upward vibration, resulting in a longer time for the particles to move to the exit. Some of the particles were unsuccessful in climbing the slope and found bouncing, which resulted in a decrease in the average velocity of the particles in the y-axis direction, as shown in Figure 7(b). Thus as the angle of inclination increases, the time for the particles to reach the outlet grows. As the angle of inclination increases, the screening efficiency decreases.

As shown in Figure 7(c), when the amplitude is 4 mm, the screening efficiency is 36.43%, which is 9.1% higher than when the amplitude is 2 mm; 8.5% higher than at an amplitude of 3 mm; 4.5% higher than the amplitude of 5mm. Therefore, it can be obtained that as the amplitude increases, the

screening efficiency of the screen will first rise to a peak and then decline. As shown in Figure 7(d), the average speed of particles in the y-axis direction increases steadily with greater amplitude. When the average speed reaches a certain value, the screening efficiency of the particles will rise, while when the average speed exceeds that value, due to the speed of the particles being too fast, the collision tally with the screen will be reduced accordingly.

As shown in Figure 8(a), when the rotational speed is 10 rpm, the screen has the maximum screening efficiency of 36.43%, while the screening efficiency of other rotational speeds is not much different compared to the screening efficiency at 10 rpm. Therefore, in equilibrium elliptical motion, the screen's rotational speed has little impact on particle screening efficiency, although there is a trend toward decreased efficiency with increasing rotational speed. As shown in Figure 8(b), As the rotational speed increases, there is a corresponding increase in the collision tally between particles and the screening surface. This is due to the fact that during the motion of particles on the screen, due to the presence of rotational motion in the screen, the particles are hit back before they can pass through the holes of the screen, resulting in an increase in the collision tally between the particles and the screen.

As shown in Figure 8(c), the screen has the maximum screening efficiency of 35.6% when the frequency is 15 Hz. The screening efficiency at 20 Hz decreased by 17.9% compared to the screening efficiency at 15 Hz; The screening efficiency at 25 Hz decreased by 23% compared to the screening efficiency at 15 Hz; The screening efficiency at 30 Hz decreased by 40.9% compared to the screening efficiency at 15 Hz. Thus, as the frequency increases, the screening efficiency of the particles decreases gradually. This is because the increased frequency accelerates particle movement along the screen's length, thereby lowering the collision tally, as shown in Figure 8(d).

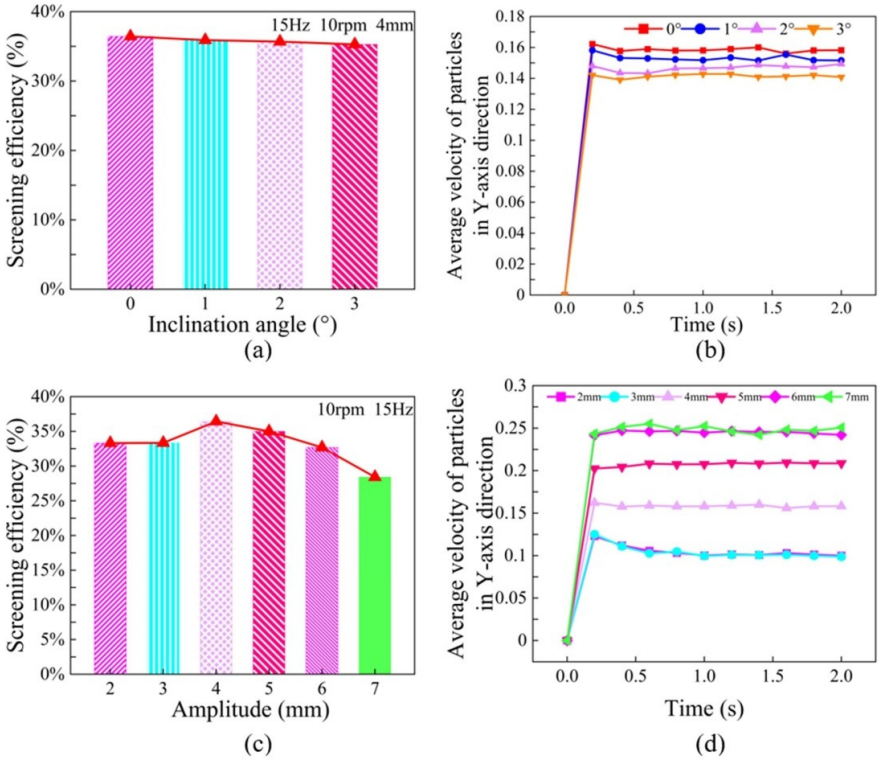

Figure 7. (a) Screening efficiency at different inclination angles; (b) Average velocity of particles in Y-axis direction at different inclination angles; (c) Screening efficiency at different amplitudes; (d) Average velocity of particles in Y-axis direction at different amplitudes.

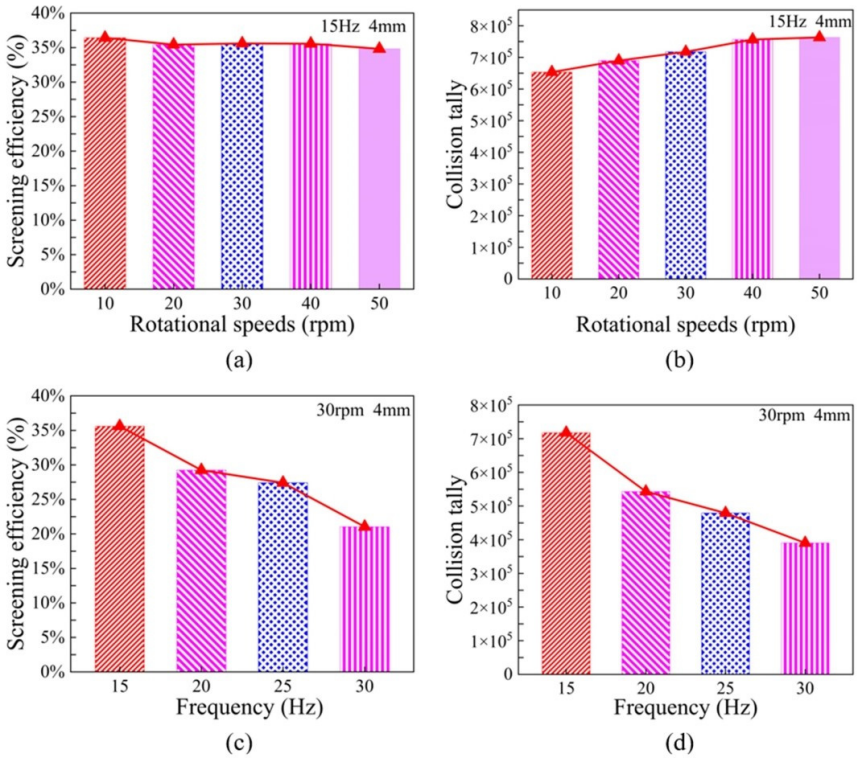

Figure 8. (a) Screening efficiency at different rotational speeds; (b)Collision tally at different rotational speeds; (c)Screening efficiency at different frequencies; (d)Collision tally at different frequencies.

(1) Effects of parameters on screening efficiency at the surface energy is 0.5 J/m².

As shown above, with higher surface energy, the average collision tally between particles and the screening surface is reduced. Particles in the vibration process, due to the existence of surface energy, have a certain amount of moisture on their surfaces, causing the wet particles to adsorb other nearby wet particles, leading to particles sticking together, which results in a decrease in particle transmission rate and a sharp decline in particle screening efficiency.

As shown in Figure 9(a), the screening efficiency is 3.84% when the amplitude is set to 6 mm, which is 75 times higher than when the amplitude is 2 mm; 1.8 times higher than at an amplitude of 3 mm; 11% higher than amplitude 5 mm; 27% higher than the amplitude of 7 mm. Therefore, it can be concluded that the screening efficiency increases gradually with the increase of amplitude, and when the average velocity of the particles exceeds a certain value, particle screening efficiency decreases markedly. The large amplitude leads to the particles being thrown to a greater height, causing them to be tossed again before they can settle into the screen. This phenomenon is similar to the trend of screen screening efficiency with amplitude at 0 j/m2 surface energy. As shown in Figure 9(b), with more amplitude, particles move faster along the y-axis. The collision count between particles and the screen shows a similar trend to that at 0 j/m2 surface energy, starting with an increase and then a decrease.

As shown in Figure 10(a), when the rotational speed is 20 rpm, the screen has the maximum screening efficiency of 2.5%, while the screening efficiency at other rotational speeds is not much different compared to the screening efficiency at 10 rpm. Therefore, in equilibrium elliptical motion, the rotational speed of the screen has little effect on the screening efficiency of particles with a surface energy of 0.5 j/m2, but there is a tendency for the screening efficiency of particles to decrease when the rotational speed is too high. As shown in Figure 10(b), with the increase of rotational speed, the number of particle-screen collisions has a different trend compared to that at 0 j/m2 surface energy. There is a gradual decrease in the number of particle-screen collisions at 0.5 j/m2 surface energy.

As shown in Figure 10(c), the screening efficiency of the screen is maximum at 2.86% when the frequency is 20 Hz. The screening efficiency at 15 Hz was reduced by 30% compared to that at 20 Hz; The screening efficiency at 25 Hz decreased by 4% compared to that at 20 Hz; The screening efficiency at 30 Hz decreased by 6.5% compared to that at 20 Hz. Therefore, as the frequency increases, the screen screening efficiency of 0.5 j/m2 surface energy particles increases first and then decreases. Since the particles have surface energy, small particles attach to larger particles. Small frequencies cannot separate the small particles from the large particles, reducing the efficiency of particle screening. With higher frequencies, particles travel more swiftly across the screen, reducing their collision frequency with the screen, as shown in Figure 10(d).

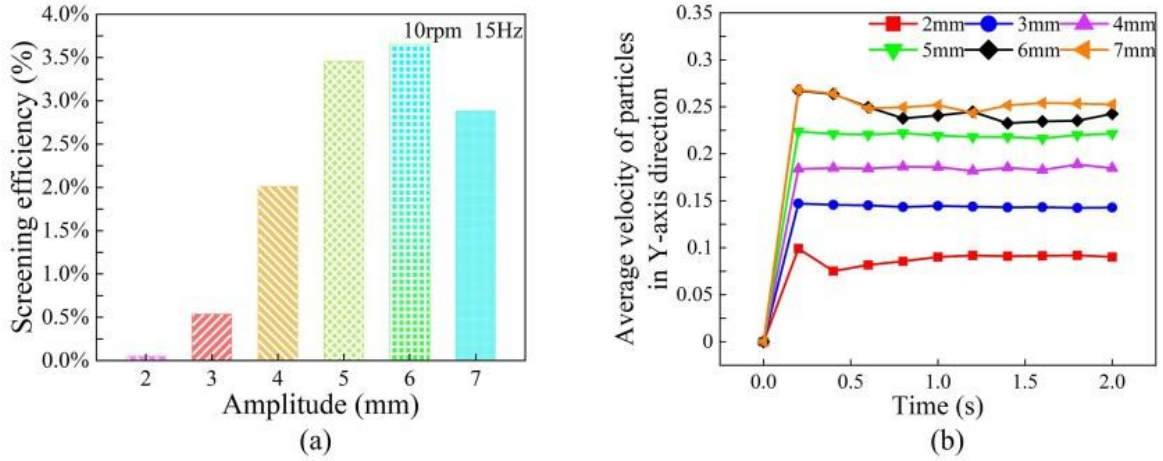

Figure 9. (a) Screening efficiency at different amplitudes; (b) Average velocity of particles in the Y-axis direction at different amplitudes.

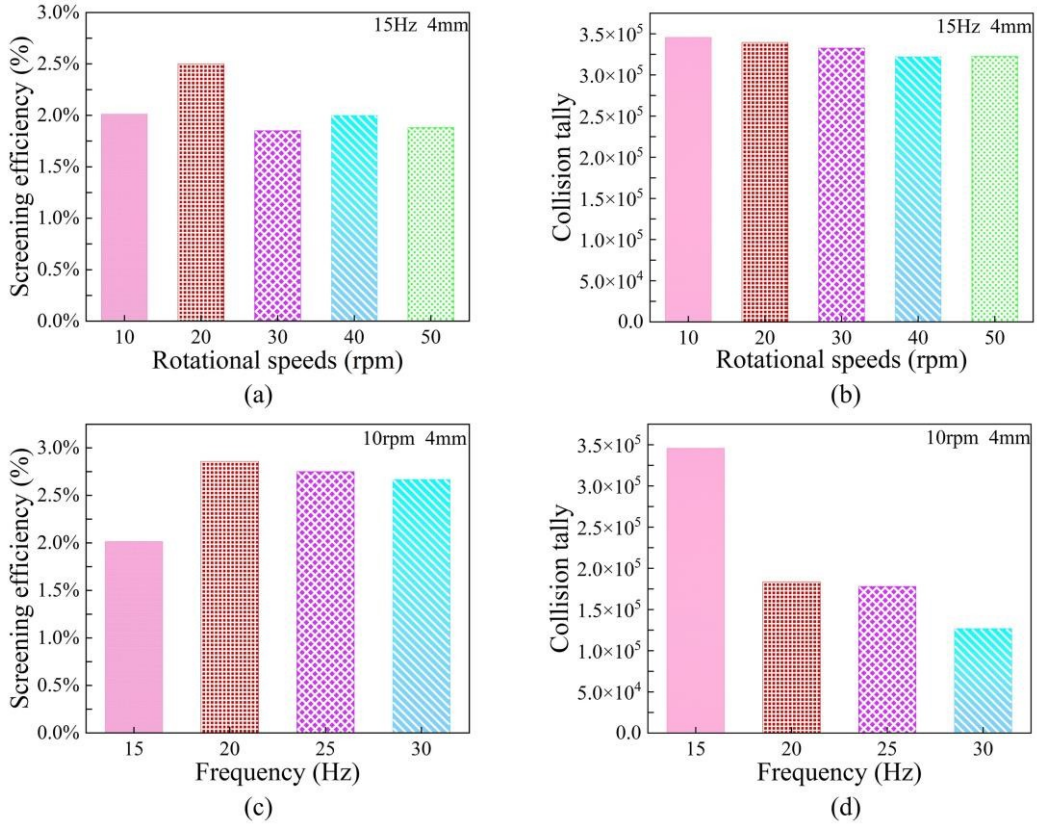

Figure 10. (a) Screening efficiency at different rotational speeds; (b) Collision tally at different speeds; (c) screening efficiency at different frequencies; (d) Collision tally at different frequencies.

4.4. Spatial Distribution of Particles Across the Screen Surface

Particles on the screen exhibit different patterns of motion and distribution under varying parameter combinations. The arrangement of particles on the surface of the screen shows the impact of each parameter on their movement. Analyzing distribution of particles provides valuable guidance for parameter optimization. The screen is divided into eight sections to analyze the distribution of particles. In this study, four representative sets of parameters were selected: (a) 15 Hz, 4 mm, 10 rpm, 0°; (b) 15 Hz, 2 mm, 10 rpm, 0°; (c) 30 Hz, 4 mm, 30 rpm, 0°; and (d) 15 Hz, 4 mm, 10 rpm, 3°.

Under parameter (a), the particles move uniformly across the screen toward the exit end and eventually exhibit an arithmetic distribution across the screen, as shown in Figure 11. At 0.87 seconds, the particles arrive at the exit end and after 1.53 seconds, they demonstrate a uniform, stepwise distribution. The particle number in the inlet area (first and second sections) ranged from 1124±48 to 1093±46. The number decreased to 984±37 in the third section and 80±20 in each subsequent section. For parameter (b), the amplitude, frequency, and speed are minimized. Due to insufficient energy, the particles do not advance or rise properly, resulting in limited interaction with the screen. The number of particles in each section exceeds 1600. The number of particles reaching the exit is small, and there is a time lag. The particles have the slowest average velocity in the y-axis direction, causing most particles to accumulate at the front of the screen.

Under parameter (c), the distribution of particles is haphazard across all sections. The distribution of particles in each section follows a fluctuating trend of rising and falling.

Consequently, small particles have difficulty passing through and exiting the outlet, which diminishes separation efficiency and throughput. In parameter (d), the amplitude, frequency, and rotational speed are the same as in parameter (a), but the screen is tilted by 3°. The distribution of particles is similar, but the inclined screen makes particle movement from the inlet to the outlet more difficult, resulting in each section of parameter (d) containing 100±30 more particles than parameter (a). Overall, efficiency improves when particles are arranged in a regular pattern on the screen. Adjustments to both the vibrating screen's structure and its parameters are essential for improving particle distribution and boosting screening efficiency. Efficient classification is achieved when particles are uniformly spread across the screen surface following smooth vibration. In cases where particles are excessively clustered at the screen's front or are moving too fast, screening efficiency will decrease, and optimal screening results will not be achieved.

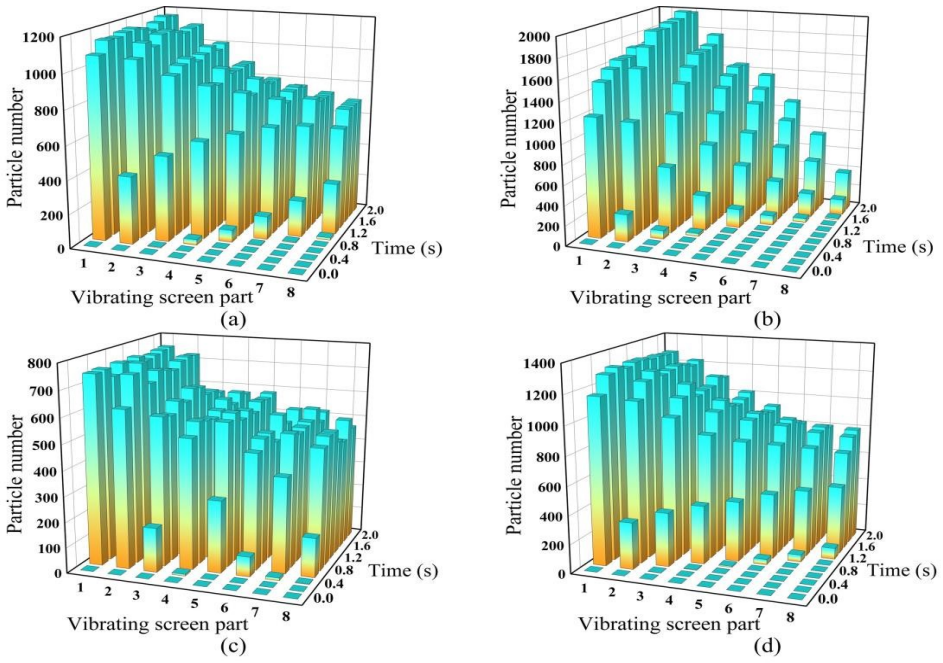

Figure 11. Distribution of particles on the screen with different parameters

5. CONCLUSION

The study simulated the behavior of wet and dry particles on A cylindrical vibrating screen that utilizes DEM for its analysis and optimization. This study examined the influence of rotational speed, amplitude, screen angle, and frequency on both screening efficiency and distribution of particles. The study evaluated the strengths and weaknesses of screening performance under different parameter settings. The summary drawn from this research are as follows:

(1) At a surface energy of 0 J/m², an augmentation in amplitude initially elevates the screening efficiency, which is subsequently followed by a decline. As rotational speed increases, the screening efficiency of the screen decreases, with a decrease trend of approximately 10% ± 3%. For each 5 Hz increase in frequency, the screening efficiency decreases by 17% ± 9%. The time for particles to move from the inlet to the outlet increases with the angle of inclination. The most effective parameter combination includes an amplitude of 4 mm, a frequency of 15 Hz, a speed of 10 rpm, and a tilt angle of 0°. At this point, the screening efficiency is more than 10% higher than with other combinations.

(2) The screening efficiency of particles is significantly reduced at a surface energy of 0.5 J/m² compared to in conditions where the surface energy is 0 J/m².The lower efficiency is attributed to the viscous forces acting on wet particles, which cause smaller particles to stick to larger ones or cluster on their surfaces, resulting in poorer screening outcomes compared to dry particles. In this study, the screening efficiency of particles with varying amplitude was similar to that of dry particles, showing a tendency to first increase and then decrease with increasing amplitude. As rotational speed increased, the screening efficiency also tended to decrease. The increase in frequency caused the screening efficiency to show a trend of first increasing and then decreasing.

(3) Particles distributed arithmetically on the screen result in higher efficiency. Screening performance is reduced under the following conditions: the inlet end of the screen has a high concentration of particles, the particles quickly advance to the outlet end, and the distribution of particles on the screen is irregular.

Future research should explore combining CFD-DEM simulations for a more accurate representation of wet particle dynamics on the screen. Given that spherical particles are an idealization, it is essential to consider a wider range of particle shapes and physical properties.

DECLARATION OF CONFLICTING INTERESTS

The authors declared no potential conflicts of interest with respect to the research, authorship, and/or publication of this article.

ORCID IDS

Yujia Li https://orcid.org/0000-0002-3765-0176

Yu Xia https://orcid.org/0009-0000-8247-5787

ACKNOWLEDGMENTS

This work was supported in part by the National Natural Science Foundation of China (52404063 and 52474004), and Chengdu Science and Technology Bureau Technology Innovation R&D Project (2022-YF05-00825-SN). (Tao Ren and Yujia Li contributed equally to this work.) (Corresponding author Yujia Li).

REFERENCES

[1] Asbjornsson, G. , M. Bengtsson, E. Hulthen and Evertsson, Model of banana screen for robust performance. Miner Eng 2016; 91:66-73.

[2] Biresaw, G. and C. J. Carriere. Correlation between mechanical adhesion and interfacial properties of starch/biodegradable polyester blends. Polymer Science, Part B: Polymer Physics 2001; 39(9): 920– 930.

[3] Chen, B. , J. Yan, Z. Yin, et al. A new study on dynamic adjustment of vibration direction angle for dualmotor-driven vibrating screen[J]. Proceedings of the Institution of Mechanical Engineers, Part E: Journal of Process Mechanical Engineering 2021; 235(2): 186-196.

[4] Chen, B. , J. W. Yan, C. L. Xu, et al. DEM simulation and experimental study on the screening process of elliptical vibration mechanical systems. J Vibroeng 2019; 21(8): 2025–2038.

[5] Cleary, P. W. Large scale industrial DEM modelling. Eng Comput 2004; 21: 169–204.

[6] Dong, H. , C. Liu, Y. Zhao, et al. Influence of vibration mode on the screening process[J]. International Journal of Mining Science and Technology 2013; 23(1): 95-98.

[7] Elskamp, F. , H. Kruggel-Emden, M. Hennig, et al. Benchmarking of process models for continuous screening based on discrete element simulations. Miner Eng 2015; 83: 78–96.

[8] Elskamp, F. , H. Kruggel-Emden, M. Hennig, et al. Discrete element investigation of process models for batch screening under altered operational conditions. Powder Technol 2016; 301: 78–95.

[9] Jiang, H. , Y. Zhao, C. Duan, et al. Kinematics of variable amplitude screen and analysis of particle behavior during the process of coal screening. Powder Technol 2017; 306: 88–95.

[10] Johnson, K. L. , K. Kendall and A. D. Roberts. Surface energy and the contact of elastic solids. Proceedings of the Royal Society of London. Series A, Mathematical and Physical Sciences 1971; 324(1558): 301– 313.

[11] Li, Y. J. , T. Ren, X. P. Meng, et al. Experimental and theoretical investigation on synchronization of a vibration system flexibly driven by two motors. ARCHIVE Proceedings of the Institution of Mechanical Engineers Part C Journal of Mechanical Engineering Science 2020; 234(13): 25502562.

[12] Li, Y. J. , T. Ren, J. N. Zhang, et al. Synchronization of two eccentric rotors driven by one motor with two flexible couplings in a spatial vibration system. Math Probl Eng 2019: 1-13.

[13] Li, Y. J, X. Fang, J. N. Zhang, System and process for mud solid control. Patent 10233707 B2, USA, 2019.03.19,

[14] Li, Y. J, P. Zhao, L. Mo, et al. Numerical simulation of particle screening efficiency of large multi-layer vibrating screen based on discrete element method. Proceedings of the Institution of Mechanical Engineers, Part E: Journal of Process Mechanical Engineering 2021; 236(2):565-574.

[15] Li, Z. F. , K. Y. Li, X. L. Ge, et al. Performance optimization of banana vibrating screens based on PSO-SVR under DEM simulations. J Vibroeng 2019; 21(1): 28–39.

[16] Li, M. , G. Z. Ma and Q. Lv. Mathematical modeling and optimization of spiral drum screen in the concrete residue recovery system. ARCHIVE Proceedings of the Institution of Mechanical Engineers. Part C: Journal of Mechanical Engineering Science 2020; 234(13): 0954406 22090794.

[17] Liao, G. W. , Y. Z. Jiang, Y. F. Hu, et al. Methods for characterizing moisture content of wet coal particles based on surface energy. China Powder Science and Technology 2021; 27(1): 71–79.

[18] Liu, C. , H. Wang, Y. Zhao, et al. DEM simulation of particle flow on a single deck banana screen[J]. International Journal of Mining Science and Technology 2013; 23(2): 273-277.

[19] Makinde, O. A. , B. I. Ramatsetse and K. Mpofu. Review of vibrating screen development trends: linking the past and the future in mining machinery industries. Int J Miner Process 2015; 145: 17–22.

[20] Ning, S. G. , J. Z. Xiao, G. F. Wang, P. C. Huang. Study on the particle stratification and penetration of a swing vibrating screen by using DEM[J]. Engineering Computations 2019; 37(3): 881-894.

[21] Safranyik, F. , B. M. Csizmadia, A. Hegedus, et al. Optimal oscillation parameters of vibrating screens[J]. Journal of Mechanical Science and Technology 2019; 33(5): 2011-2017.

[22] Shanmugam, B. K. , V. Harsha, R. M. Govinda, K. Marutiram, S. Rameshwar, H. Harish. Screening performance of coal of different size fractions with variation in design and operational flexibilities of the new screening machine[J]. Energy Sources, Part A: Recovery, Utilization, and Environmental Effects, 2023, 45(2): 4361-4369.

[23] Steffen, S. , A. Ermek and R. Benjamin, et al. Modelling of partially wet particles in DEM simulations of a solid mixing process. Powder Technology 2018; 338: 354–364.

[24] Tang, H. , Y. Jiang, J. Wang, et al. Numerical analysis and performance optimization of a spiral fertilizer distributor in side deep fertilization of a paddy field. Proceedings of the Institution of Mechanical Engineers, Part C: Journal of Mechanical Engineering Science 2020; 235(18):3495-3505

[25] Wang, Z. Q., L. P. Peng, C. L. Zhang, L. Qi, C. S Liu, Y. M. Zhao. Research on impact characteristics of screening coals on vibrating screen based on discrete-finite element method[J]. Energy Sources, Part A: Recovery, Utilization, and Environmental Effects, 2020, 42(16): 1963-1976.

[26] Wu, J. D. , C. S. Liu, H. S. Jiang, B. Zhang. A vibration-test-based calculation method of screening material mass of a mining crank-link type flip-flow screen[J]. Energy Sources, Part A: Recovery, Utilization, and Environmental Effects, 2024, 46(1): 9655-9675.

[27] Wu, X. Q. , Z. F. Li, H. H. Xia, et al. Vibration parameter optimization of a linear vibrating banana screen using DEM 3D simulation. Journal of Engineering & Technological Sciences 2018; 50(3): 346–363.

[28] Xu, N. , C. Yu, S. Gong, et al. Numerical study and multi-objective optimization of flexible screening process of flip-flow screen: A DEM-FEM approach[J]. Advanced Powder Technology 2022; 33(7): 103650.

[29] Yang, J. , W. Zhang, J. Gao, et al. Optimizing RAP sieving efficiency of linear vibrating sieve using DEM simulation[J]. Construction and Building Materials 2022; 333: 127442.

[30] Yin, P. , Y. J. Hou, X. J. Wu. Simulation of particles screening in pulsating negative pressure shale shaker by coupling CFD and DEM[J]. Engineering Computations 2022; 39(5): 1701-1722.

[31] Yin, Z. J. , H. Zhang, T. Han. Simulation of particle flow on an elliptical vibrating screen using the discrete element method[J]. Powder Technology 2016; 302: 443-454.

[32] Zadravec, M. , B. Orešnik, M. Hriberšek, et al. Two-step validation process of particle mixing in a centrifugal mixer with vertical axis. ARCHIVE Proceedings of the Institution of Mechanical Engineers, Part E: Journal of Process Mechanical Engineering 2018; 232(1): 29–37.

[33] Zhai, Y. X. , X. Y. Xiong and J. Tang. Impact disaggregation simulation of wet coal agglomerate using discrete element method. Coal Eng 2019; 12(51): 167–171.

[34] Zhao, La. La. , Y. M. Zhao, C. Y. Bao, Q. F. Hou, A. B. Yu. Optimisation of a circularly vibrating screen based on DEM simulation and Taguchi orthogonal experimental design[J]. Powder Technology 2017; 310: 307-317.

[35] Zhao, L. L. , Y. M. Zhao, C. Bao, et al. Optimisation of a circularly vibrating screen based on DEM simulation and Taguchi orthogonal experimental design. Powder Technol 2017; 310: 307–317.

[36] Zhong, W. Q. , A. B. Yu, X. J. Liu, et al. DEM/CFD-DEM modelling of nonspherical particulate systems: theoretical developments and applications. Powder Technol 2016; 302: 108–152.

[37] Zhu, H. P. , Z. Y. Zhou, R. Y. Yang, et al. Discrete particle simulation of particulate systems: a review of major applications and findings. Chem Eng Sci 2008; 63: 5728–5770.